Interaction of inter- and intralaminar damage in scaled quasi-static indentation tests: Part 1 - Experiments

E. Abisset[a], F. Daghia[a], XC. Sun[b*], M.R. Wisnom[b], S.R. Hallett[b]

[a] LMT-Cachan/ENS-Cachan/CNRS/Université Paris Saclay, 61 av. Du Président Wilson, 94235 Cachan CEDEX, France

[b] Advanced Composite Centre for Innovation and Science (ACCIS), University of Bristol, Queens Building, University Walk, Bristol BS8 1TR, UK

Abstract

The evaluation of the predictive capabilities of models proposed in the literature for laminated composites calls for experimental testing providing detailed results of both the global and local response in terms of degradation mechanisms, such as delamination, transverse cracking and fibre breaking. Scaled tests, in which one or more characteristic dimensions are modified, allow variation of the different mechanisms. In this paper, a unique series of scaled indentation tests are performed on quasi-isotropic composite plates, and a detailed assessment of the damage evolution is carried out through non-destructive techniques, including ultrasonic C-scan and X-ray Computed Tomography (CT). Four different configurations are tested, presenting changes in both in-plane dimensions and fully three dimensional scaled cases. The latter are performed with sublaminate and ply scaling to show the effect of ply thickness on response. A detailed set of results for both global behaviour and the damage evolution is provided to demonstrate the mechanisms controlling behaviour and to create a reference set of data for model validation. The scaling effects observed are also discussed making use of simplified analytical models.

Keywords: Laminates, Static indentation, Impact damage, Mechanical testing, Analytical modelling

* Corresponding author
E-mail address: Ric.Sun@bristol.ac.uk (Xiaochuan Sun)

1. Introduction

In the last decade, the increased use of laminated composites in advanced structural applications has required the development of a wide variety of modelling strategies for the description of composite materials and structures. The validation of the predictive capabilities of such models for damage becomes a real challenge, which needs to be addressed if these strategies are to be introduced in industrial practice.

In order to be used for virtual structural testing, that is for numerical simulations dedicated to the design of laminated structures, a model must be able a priori to predict structural failures in a wide range of complex loading cases. A first task is to define the degradation mechanisms that are involved. Structural failure originates from two main mechanisms: fibres breaking within the plies or delamination between plies. However, other subcritical degradations may play an important role in the final failure. In particular, intralaminar cracks, generally appearing at relatively low stress levels, have been shown to act as initiators for delamination [1–3] or to reduce stress concentrations associated with holes and notches to delay fibre failure [4]. Depending on the relative importance of each mechanism, the final failure scenario and the associated load may change significantly. Thus, tests chosen for validation of the models should highlight the different interactions between the following main degradation mechanisms: intralaminar cracks, delamination and fibre fracture.

A simple way of disrupting the failure sequence between these elementary degradation mechanisms, and thus of exploring a wide variety of failure scenarios with little or no change in the experimental setup, is the use of scaled tests. The principle is to perform a series of experiments using the same setup but varying the characteristic geometrical parameters, such as ply thickness or in-plane dimensions of the sample as well as the dimensions of the experimental apparatus. As the degradation mechanisms do not depend in the same way on these characteristic parameters, a modification can change the failure scenario for the same experimental setup.

This idea has already been applied, for example, to open-hole tensile tests on quasi-isotropic laminates [5]. A wide range of laminates made of the same material and stacking sequences was tested. The tests have shown that a simple change in the ply thickness led to a dramatic difference in the failure scenario, from fibre-dominated to delamination-dominated failure. Furthermore, the variation of strength with in-plane dimensions followed an opposite trend in the case of each failure scenario. This experimental work was used both by the authors and by other research groups [6–10] as a basis for validation of different proposed models.

The objective of this work is to apply the idea of scaled tests e.g. [11] and [12] to a quasi-static indentation test configuration with close similarities to the low-velocity impact test of the ASTM D7136 standard [13] in terms of test configurations and damage mechanisms involved. Many works on low-velocity impact and static indentation test presented in the literature generally focus on a single simple geometry and do not emphasise the acquisition of comprehensive results in terms of damage evolution prior to final failure. In this paper, the authors provide extensive results for scaled indentation tests which highlight the fundamental controlling mechanisms. These are then used to validate numerical models in part 2 of this study. The experiments are also documented in sufficient detail in order to provide a reference for model validation for other researchers.

In [14], low-velocity impacts are defined as impacts in which the contact time between the impactor and the plate is long enough to allow all wave reflections from the boundaries. The relation between deflection and impact load approach those of a purely static loading case [15]. In terms of validation, however, low-velocity impact tests do not allow one to observe the succession and evolution of the degradation mechanisms within the plate, since the plate can only be inspected upon the completion of impact testing. For this reason, a number of researchers have turned their attention to static indentation tests. These tests have been demonstrated to give similar global behaviour and damage states as low-velocity impact tests

[16–19]. Since they are static tests, they can be easily interrupted at different stages to observe the damage evolution within the plate. Figure 1 shows X-ray images comparing two identical composite laminates having a similar projected delamination area induced by quasi-static indentation and dynamic low-velocity impact. No obvious difference can be detected in terms of damage morphology.

Extensive studies can be found in the literature involving experimental results for low-velocity impact or static indentation tests on laminated composites. A few of these works are reviewed here, to illustrate the existing results and to motivate the proposed experiments in this work. In the experiments described in the literature, the plate is often a circular or a rectangular shape; it is either clamped between two fixtures or simply supported on a steel window (see Section 2.1 for more details). In most cases, quasi-isotropic lay-ups are considered [19–22], while some works deal with cross-ply $[0_n/90_m]_S$ or $[0_n/45_m]_S$ stacking sequences [23,24]. The results reported are varied but can be classified into two main categories. On one hand, some papers explore the scaling effect as defined before [22,25,26], but in this case exhaustive experimental data on all the degradation mechanisms are not given, with results generally being limited to the global responses or overall damage extent [24,27]. On the other hand, there are studies focusing on a specific feature of the response, such as the delamination threshold [28,29] or the local indentation effect [21,30]. However, papers reporting complete results in terms of global response and damage evolution together are rare, and mostly concentrate on a single lay-up and material configuration. Since both the experimental parameters and the available information on the plate response vary largely from one paper to another, it is difficult to draw conclusions on the scaling effects in these types of test.

As shown in Figure 2, in terms of global response in most of the described tests, the plate experiences three loading stages during transverse out-of-plane loading. The response involves different damage mechanisms, and the transition of each stage is associated with one or multiple significant load drops. At the beginning, Stage I shows an elastic response, however nonlinear behaviour appears, which can be attributed to local

indentation effects, matrix cracking and geometrical nonlinearity. When the load reaches a critical value F_C indicating delamination onset, a large load drop occurs, followed by the response with degraded global stiffness ($K_{II} < K_I$) in Stage II. With propagation of the underlying delamination in Stage II, the degree of nonlinearity increases, with multiple delaminations, and eventually leads to fibre failure at the bottom and top of the specimen as the load increases in Stage III [19,24,27,30], after which complete penetration will take place, which was not considered in this study.

In this work, the objective is to obtain a detailed description of the evolution of the damage during static indentation. Scaled static indentation tests are performed and non-destructive inspection techniques are used to evaluate the damage scenarios within the plates at different load levels.

2. Experimental Method

2.1. Definition of the test cases

Different configurations are used in the literature for low-velocity impact and quasi-static indentation tests, ranging from circular to rectangular specimens, which are either fully clamped or simply supported [31,32]. In the aerospace industry, an accepted test configuration is a rectangular 150 × 100 mm specimen, simply supported on a 125 × 75 mm window with four rubber-tipped clamps, as per the ASTM D7136 standard [13]. This configuration is used and scaled in this work, and a schematic of it is presented in Figure 3.

Similarly to the open-hole tensile tests studied in [1], in this paper the focus is on two types of scaling: in-plane scaling and thickness scaling. In order to keep reasonably-sized specimens, the original 150 × 100 mm plate, support window and indenter are downscaled by a factor of two to obtain the Reference specimen (termed ‘Ref’ hereafter). In-plane scaling (hereafter termed ‘Is’) is achieved by having the same thickness as the Ref case, but with double the in-plane dimensions. Three-dimensional scaling is achieved by doubling both the in-plane dimensions and the plate thickness.

A quasi-isotropic stacking sequence, $[45_m/0_m/90_m/-45_m]_{ns}$ (where 0 is the direction of unidirectional fibre orientation parallel to the long side of the plate), is chosen for all specimens. The specimen thickness can be doubled either by doubling 'm' (ply-block scaling, hereafter termed 'Ps') or by 'n' (sublaminate level scaling, hereafter termed 'Ss'). This scaling was expected to play a role in damage development, since the propensity for transverse cracking and delamination is dependent on ply block thickness, as observed in some literature results [20,22,23]. It should be noted that in this case, due to the choice of the quasi-isotropic stacking sequence, the overall flexural stiffness of the Ps and Ss configurations is extremely similar allowing an easy comparison between the global load-displacement curves. The characteristics of the tested specimens are summarised in Table 1.

2.2. Material and methods

The specimens were made using Hexcel IM7/8552 unidirectional pre-impregnated sheet with 0.125 mm nominal cured ply thickness. The manufacturer's recommended curing cycle was used and mechanical properties can be found in [8]. Static indentation tests were conducted by mounting a 16 mm (or 8 mm for Ref case) diameter steel tup to an INSTRON servo-hydraulic testing machine. This indenter was forced against the specimen which is simply supported over a 125 × 75 mm (or 62.5 × 37.5 mm for Ref case) window as shown in Figure 3. The indentation tests were conducted under displacement control at a rate of 0.5 mm/min for all cases. The dynamic and rate effects of laminate were considered to be eliminated at this slow loading rate. The load and displacement of the indenter of the test was acquired at a sampling rate of 20Hz. When the desired milestone (e.g. just before or after the first significant load drop), was achieved during the test, the specimen was then unloaded. Ultimate failure is defined by the development of fibre breakage in the lower plies shown as multiple load drops at Stage III in Figure 2.

In order to follow the evolution of the degradation mechanisms during the tests, nine coupons were manufactured for each test case and the following interrupted tests performed:

- 3 specimens were loaded until ultimate failure in order to evaluate the repeatability of the test and to determine the load level of each load drop.
- 1 specimen was loaded and interrupted just before the first significant drop in the load curve (as pre-determined from the complete failure tests above).
- 2 specimens were interrupted just after the first load drop.
- 3 specimens were interrupted at different load levels between the first load drop and the final specimen failure load.

In order to describe and understand the relation between the different damage mechanisms occurring extensive Non-Destructive Inspection (NDI) was carried out; ultrasonic C-scan for overall damage mapping and X-ray Computed Tomography (CT) scanning for full 3D damage interpretation.

3. Experimental Results

3.1. Global behaviour

Typical load-displacement curves associated with the four types of specimens are plotted in Figure 4. Apart from the obvious differences in stiffness, related to the different thickness and in-plane sizes of the plates, all four curves display a similar global behaviour. This is characterised by a first load drop, occurring long before final failure, followed by significant load recovery of the specimen up to more than twice the magnitude at the load drop. Once a second threshold is reached, a series of damage events generate a number of subsequent load drops. The tests were stopped as soon as fibre failure in the lower ply was observed.

The repeatability of the tests was verified by superimposing the load-displacement curves for all the specimens, and also by comparing the force at the first load drop. In Ref, Is and Ps cases, the maximum variation was found to be around 5 to 6%, while it was even lower (1.3%) for the Ss case, showing a very good repeatability for all tests.

A number of characteristic features were measured for all tests; the critical load (F_C) and the displacement corresponding to the first load drop, percentage of the load drop, the maximum transverse crack length

before the load drop and the delamination size after the load drop. These values are reported in Table 2 and discussed in the next section. The force and displacement values at the first load drop, as well as the size of the load drop itself, appear to scale in a non trivial way with the plates' in-plane and thickness dimensions. In particular, the size of the load drop was found to be much more significant (around 20%) for thick plates, while it could nearly be overlooked for thin ones. A more detailed investigation of the damage development in the plates, reported in the next section, focuses on the events before and after this first load drop.

3.2. Damage evolution

Non-destructive evaluation of the damage in terms of transverse cracks and delamination was systematically carried out for each interrupted specimen. An overall evaluation of the delaminated area was achieved via C-scan, performed for each interrupted test on both sides of the plate. More detailed information on the presence of matrix cracks and the shape and size of delamination at each interface was obtained via CT-scan. Prior to CT-scan, a small hole was carefully drilled at the centre of the local permanent indentation in order to introduce zinc-iodide penetrant, used to highlight the presence of cracks and delamination.

3.2.1 C-scans: global evolution of the delamination

Figures 5-8 display the load-displacement curves for each case, as well as the C-scan images obtained for some of the interrupted specimens at both indented (front) face and back face. In particular, the time-of-flight information from C-scans was colour coded to depict the delamination at different interfaces. The values are not presented here since the C-scans are only employed here to obtain an overall evaluation of the projected delaminated size.

No delamination could be observed in any of the C-scans preceding the first load drop. However, transverse cracks within the plies were observed in the CT-scans that could not be detected by the C-scans. Significant delamination was systematically observed after the load drop. This first drop appears thus to be caused by

initiation and immediate propagation of delamination at a number of different interfaces. Some of these delaminations can be seen to have further propagated in the C-scans taken after the second load drop. The overall size of the delamination after the first load drop, accessed by CT-scans, is taken as a characteristic feature of the plate damage and reported in Table 2.

3.2.2 CT-scans: detailed damage mechanisms for each ply and interface

The CT-scans carried out on the specimens interrupted before the first load drop confirm the presence of damage in the form of intralaminar cracks in all plate configurations. As could be expected, these cracks are located in the bottom part of the plate (that is, in the zone which is under tension during testing). In the case of the thin plates (Ref and Is), all the plies in the bottom half of the plate are involved, while in the case of the thick plates (Ps and Ss) cracks appear only in the bottom quarter of the plate. Most of the cracks are localised in a very limited zone around the indenter, while in the bottom 45◦ ply the longest cracks were found. Comparisons between the different tested configurations for the uppermost transverse cracks and for the cracks in the bottom ply are given in Figure 9 and Figure 10. The maximum length of the transverse cracks at the bottom of the plate before the first load drop is taken as a characteristic feature of the plate damage and is reported in Table 2.

The CT-scans carried out on the specimens interrupted after the first load drop give detailed information on the delamination and transverse crack patterns within the plates. These data are extensive and can not all be included in this paper. Overall views of the damage pattern for each case are given in Figure 11, while some characteristic interfaces are extracted and compared across the test cases in Figure 12 and Figure 13. The full comparison of damage in all the interfaces is available for download from the Research Data Repository of University of Bristol at data.bris.ac.uk/data/dataset/12gx6827n337u1dxy6iilf3t1f.

The delamination pattern appears to have a similar shape in all the plate configurations. Two delaminations, symmetrically positioned with respect to the indenter, develop at each interface, their shape and orientation

determined by the fibre directions in the adjacent plies. Triangular shaped delaminations develop between plies whose fibre directions are different by 45^o (see for example the top 90/ −45 interfaces in Figure 12), whereas delaminations shaped as half-circles develop at 90^o interface where fibre directions are different by 90◦ (see for example the bottom 90/0 interfaces in Figure 13). In all cases, transverse cracks parallel to the fibre direction develop within the plies and allow the delaminations at the different interfaces to join up. The overall projected delaminated area has a circular shape and, thus, it is most effective in decreasing the plate flexural stiffness and releasing the stored elastic energy. Similar observations have been made in previous works on impact damage, mostly from C-scan results. While the shape of the delaminations appears similar in all four test cases, their size scales in a non-trivial way (as was anticipated when looking at the C-scans). It is thus also taken as a characteristic feature of the plate damage and reported in Table 2.

3.2.3 CT-scans: Interaction between intralaminar cracks and delaminations

From the X-ray CT-scan on damaged specimens after the first load drop it was seen that individual delamination development is significantly influenced by the matrix cracks in its neighbouring plies. Figure 14 provides a set of CT-scan images showing individual delamination shapes at damaged interfaces for the Ps case interrupted after the first load drop. The major matrix cracks are highlighted using dashed lines.

Several common damage behaviours of the tested composite laminates can be summarised as follows from this damage assessment, which confirm other conclusions made in the literature [21,33,34] and are also predicted in the proposed high-fidelity models in part 2 of this study [35].

- Due to matrix plasticity and damage, a permanent indentation is seen at the top ply in direct contact with the indenter.
- Delamination propagates at each interface between dissimilar fibre plies except the first interface (top $45^o/0^o$ interface), believed to be due to the high contact stress immediately under the loading site. No delamination is found at the interface between blocked plies with the same fibre orientation.

- Delaminations always propagate along the direction of the lower ply fibre orientation, and propagation normal to the fibre direction is impeded by matrix cracks. The delamination area is smaller between plies with a 45^o orientation difference (45^o interface) than between plies with a 90^o orientation difference (90^o interface).
- A 'delamination-free' zone is observed underneath the contact site in the through-thickness direction due to the high compressive stress [36] from Hertzian contact stresses, which supresses the delamination formation.
- Delamination at 45^o interfaces propagates in a triangular shape which is intersected by two pairs of long matrix cracks.
- There is at least one pair of long matrix cracks formed where the delamination starts to propagate, and no delamination is found within the area between the long matrix cracks.
- Multiple matrix cracks due to tension can be found in the lower sublaminate groups.

4. Scaling Effects

The experimental results presented show that a similar sequence of damage events occurs in all configurations. However, the scaling of the characteristic quantities appears to be quite complex, since it is related to the occurrence of different damage mechanisms, which are governed by the plate in-plane and thickness dimensions. Although the main aim of this paper is to provide detailed experimental results for model validation in part 2 [35], in this section it is attempted to give some preliminary interpretations of the main scaling effects observed, based on simplified analytical models

4.1. Initial stiffness scaling

Even when considering only the linear elastic response, flexural tests are more complex to compare than tensile tests (such as the ones considered in [1]). Since the material is inhomogeneous, and it is not possible

to present the local averaged stress/strain relation, the scaling of the initial flexural stiffness with the plates dimensions must be considered if the results are to be compared.

Table 3 shows the comparison of experimental and analytical initial stiffness for each case. The analytical initial stiffness is calculated by the expression $E_{eff}h^3/\eta b^2$ from [37], where E_{eff} is the effective homogenized Young's modulus of the laminate, h and b are the thickness and the characteristic dimension (the unsupported width of the opening in this case) of the laminate. η=0.175 here is a correction factor which depends on the aspect ratio of the plate [17]. The lower estimation of the analytical solution in the Ref and Ps cases is because the local indentation effect is not accounted for. According to the above expression and plate theory for both quasi-isotropic and isotropic material, the plate flexural stiffness is proportional to h^3/b^2 [38]. The stiffness of the Ps and Ss plates should thus be double that of the Ref plate, since both thickness and in-plane dimensions are doubled, while the stiffness of the Is plate should be one-fourth that of the Ref plate, since only the in-plane dimension is modified. This scaling appears to agree reasonably with the slopes measured for the Ref, Ps and Ss cases as shown in Table 3. The scaling parameter is the h^3/b^2 value of each case normalised by that of the Ref case. Here, the slight difference between the experimental stiffnesses of the Ps and Ss plates is attributed to the difference in the individual ply thicknesses. The lower estimation in the Is case is caused by the strong non-linearity at the very beginning of the experimental load-displacement curve shown in Figure 4 that can be explained by the membrane stiffening effect.

In order to understand the importance of nonlinear effects in the scaled plates, the behaviour of these four scaled specimens under static indentation can be simplified as a spring-mass model up to the critical load, if one ignores the local indentation due to Hertzian contact stresses. The above expression for the initial stiffness can be expanded into the following form based on thin circular plate theory,

$$F = k_{bs}\omega_o + k_m\omega_o^3 \quad \text{where } k_{bs} \approx \frac{E_{eff}h^3}{\eta b^2} \quad k_m \approx \overline{k}_m \frac{E_r h\pi}{4b^2} \tag{1}$$

where F and ω_o are the force and the mid-plane out-of-plane deflection, k_{bs} and k_m are the bending-shearing stiffness and membrane stiffness of the plate, $\overline{k}_m$ = 0.157 is a dimensionless factor determined by the boundary conditions and mobility of the plate [37]. The bending stiffness term, k_{bs}, is a function of the effective homogenized Young's modulus of the laminate (E_{eff}), the thickness, h, the width of the unsupported opening b (75mm for the large plates and 37.5mm for the Reference plate) and a constant η. The membrane stiffness term, k_m, is proportional to, E_r, the effective in-plane Young's modulus and h/b^2. If one compares the first linear term associated with bending-shearing stiffness with the second nonlinear term, the second term is small enough to be neglected for a small deflection. The deflection then becomes a linear function of contact force F through bending-shear stiffness, which is observed in all cases except the Is case. The load-displacement curves derived from analytical solution (Eq. 1) and the experiment are compared in Figure 15(a), It is can be seen that the correlation between the test result and the linear analytical solution before the first load drop is very good in the case of the Ps and Ref plates, but a significant difference is found in Is case.

The special case of the Is plate is that it has a halved thickness to width ratio (h/b) thus h^3/b^2 is much smaller than for the other plates, making the nonlinear membrane term that is associated with ω_o^3 greater with increasing deflection and approaching the same order of magnitude as the linear bending-shear term. Figure 15(a) also shows a comparison between the analytical solution with and without the nonlinear term that is associated with the membrane stiffness for the Is case. Using only the first linear term of the expression is no longer accurate to represent the response of Is plate. The nonlinear term $k_m\omega_o^3$, in this case, dominates the overall plate response, showing a strong nonlinearity in the load-displacement curve.

After the load reaches a critical value for all cases, the nonlinearity of the response is further increased because the delaminated portion acts as multiple thin plates. As the number of delaminations increases and the size of the delaminations becomes larger, so the nonlinear response becomes more significant [39]. With increased loading, the degradation of flexural stiffness due to the damage is counteracted by the membrane stiffening effect at the large deflections, particularly for the Is case.

The Ps case can be treated as a true scaled-up replica of the Ref case since all geometric parameters [40] of both are satisfied with a scale factor $\lambda = 2$ according to the Pi theorem [41]. Therefore, the contact force and deflection of the Ref case should be scaled up by λ^2 and λ respectively to replicate the response of the Ps case. The comparison made in Figure 15(b) shows that the scaled Ref plate result indeed correlates with the Ps test results very well in terms of initial stiffness, degraded stiffness and even the number of load drops, which once more confirms that the damage mechanism of both is very similar. However, each load drop in the Ps case occurs at a significantly lower load than for the scaled Ref case. This is because the damage initiation and critical load are in fact not able to be accurately scaled with simple similitude laws, as discussed in the next section.

4.2 First load drop scaling

As discussed in Section 3.2.1, the first load drop is caused by initiation and immediate propagation of delamination at a number of different interfaces. Different characteristic features of this load drop have been pinpointed when discussing the experimental results:

- the maximum force before the load drop (or critical load ~ F_C)
- the percentage of the reduction in load at the first load drop
- the projected delamination size after the first load drop

An interpretation of the scaling of these quantities requires the understanding of the mechanisms associated with the delamination propagation within the composite plates.

Simple analytical models to predict the main features of delamination propagation within a plate loaded by a central transverse load have been proposed in the literature [39,42–44]. Similar to the previous expression shown in section 4.1, the authors considered a circular isotropic plate with clamped boundary conditions under a central point loading, and the load-displacement relation of the plate was based on the theory of thin plates. They studied the loading condition to propagate a representative single circular delamination located at the mid-plane of the plate [42] , or a number (N−1) of circular delaminations which are equally spaced through the plate thickness, dividing the plate into N sublaminates, in linear [43] and geometric nonlinear [39] regimes. Notwithstanding the many simplifications, these models are useful for a first evaluation of the expected dependence of the plate behaviour on its characteristic dimensions. The linear model [43] predicts that the propagation of delamination takes place at a constant load $F_D$which depends on the plate's material and geometrical parameters, as well as on the number of circular delaminations. The general expression for N-1 delaminations as given in [43] is:

$$F_D = \sqrt{\frac{32\pi^2 D G_{IIC}}{N+1}} \qquad (2)$$

where $D = \frac{E_{eff} h^3}{12(1-\nu^2)}$ is the equivalent bending stiffness, N is the number of sublaminates, and G_{IIc} is the mode II critical strain energy release rate. The expression given in [42] for a single delamination can be found as a particular case of Eq. 2, with N=2.

The geometrically nonlinear model [39], on the other hand, predicts that propagation at (nearly) constant load can only occur up to a certain delamination size; after that, the geometric nonlinear effect starts to become important and the load needs to be increased in order to obtain further delamination growth.

The energy condition given by Eq. 2 only accounts for crack propagation, however a stress-based condition for initiation should also be satisfied in order for the delamination to occur. Before the first load drop, the

maximum shear stress associated with the plate bending occurs at the mid-plane of the plate. Therefore a single central delamination is expected to initiate at this location. For this reason, Eq. 2 with N=2 is expected to give a reasonable approximation of the force value, F_C, at which the first load drop occurs. Migration of this central delamination from its initial interface to different adjacent interfaces through transverse matrix cracks (as observed in the experimental results) creates a damage morphology comparable to that of a full circular area of multiple delaminations, as assumed in the simplified analytical models.

The stress redistribution associated with the propagation of a mid-plane delamination increases the shear stress at the mid-planes of the newly created sublaminates, enabling the initiation of further delaminations. According to Eq. 2, increasing the number of delaminated interfaces decreases the load associated with propagation. The unstable initiation and propagation of multiple delaminations is interpreted to be the cause of the load drop. For laminates with $N > 2$ number of sublaminates at the end of unstable initiation and propagation of multiple delaminations (i.e. N -1 > 1), the force just after the load drop can be given again by Eq.2. N=4 was selected for the Ref and Ps cases according to their laminate configurations, and it is consistent with the analytical studies available in the literature [39,43,45]. The expression of the displacement given in [43] for a circular homogeneous plate can then be used to estimate the size of the delamination just after the load drop.

The numerical values of the critical load, percentage of load drop and delamination size estimated using this simplified model are given in the following Sections. While in most cases the orders of magnitude appear reasonable, this extremely simplified analysis cannot capture all of the key features of the response. In particular, geometric nonlinearity should be introduced in order to account for the force increase after the first load drop and to improve the description of the behavior of the thin plates (Is, and also to a lesser extent Ref). A way to account for the effect of geometric nonlinearity in a simplified analytical formulation was recently proposed in [45]. Alternatively, full Finite Element simulations accounting for geometric

nonlinearity, as well as the progressive damage development, were carried out in part 2 of this work [35]. The sequence of damage mechanisms proposed in this simplified analysis (initiation and propagation of a central delamination, immediately followed by unstable initiation and propagation of multiple delaminations) was confirmed by the numerical results.

4.2.1 Force associated with the propagation

Estimates of the theoretical force associated with the propagation of a single, circular mid-plane delamination (i.e. N-1=1) can be obtained from Eq. 2 using effective mechanical properties and the critical energy release rate. Since the plates are not isotropic and they are subjected to flexural loading, the minimum equivalent flexural modulus and associated Poisson's ratio are used in the calculation. The critical strain energy release rate in mode Mode II is taken from [32]. The input values and predicted propagation loads are reported in Table 4. These theoretical estimates capture reasonably well the magnitude of the forces associated with the first load drop for all plates. Because the effects of ply thickness and in-plane dimensions are not taken into account in Eq. 2, the predictions are not highly accurate.

Looking at the predicted values in more detail, one can notice that, in three out of four cases (namely, the Ref, Ps and Ss plates), the loads are overestimated. This could be associated with the presence of transverse cracks prior to delamination; these cracks, indeed, help the occurrence of delamination by creating stress concentrations at the interfaces. In the Ps case, the thicker ply blocks lead to less resistance to transverse cracking prior to delamination, and the overestimation is more significant than in the Ss case. In Eq. 2 the predicted critical load is independent of the plate in-plane dimensions, hence the estimates of the Ref and Is plates have the same value of 1.61 kN. The underestimation of the critical load in the Is plate can once again be attributed to the more significant geometric nonlinear effects on the whole plate, as discussed previously.

4.2.2. Size of the load drop

As discussed in Section 4.2, the load drop is expected to be caused by the initiation and propagation of multiple delaminations, which immediately follow the first central delamination. An estimate of the load drop value for the perfectly scaled Ref and Ps cases can be obtained by considering N=4 according to their laminate configurations. This yields

$$\Delta F = \sqrt{\frac{32\pi^2 D G_{IIC}}{3}} - \sqrt{\frac{32\pi^2 D G_{IIC}}{6}} = \sqrt{\frac{32\pi^2 D G_{IIC}}{3}}\left(1 - \frac{1}{\sqrt{2}}\right) \approx 0.26 F_C \qquad (3)$$

where F_C is the force value just before the load drop. Compared to the experimental values in Table 2, Eq. 3 appears to give a reasonable estimate of the load drop for the thick Ps plate, while it greatly overestimates the experimental response for the thin Ref plate. The expected reason is once again the effect of geometric nonlinearity. The local nonlinear effects in the delaminated region might be expected to be more significant for thin plates than for thick ones (see [45]).

Observing the results from Table 2, indeed, it appears that the level of the load drop is related to the overall thickness of the given laminates. The same observation has been found in similar tests in the literature [46,47].

4.2.3 Scaling of damage size

The simplified model proposed in [43] can also be used to estimate the size of the delaminated area right after the load drop, under the same plate and boundary condition assumptions as in section 4.2. One can start from the expression for the mid-plane displacement (ω_0) of the plate centre, given as

$$\omega_0 = \frac{FR^2}{16\pi D}(1 + (N^2 - 1)\alpha^2) \qquad (4)$$

where R is the radius of the circular plate and $\alpha = a/R$ is the nondimensional delamination radius. In the displacement driven test, the value of ω_0 before and after the load drop are the same. One can then write

$$\frac{F_C R^2}{16\pi D} = \frac{F_{C\_2} R^2}{16\pi D}(1 + 24\alpha^2) \quad (5)$$

where F_{C_2} is the force at the end of the unstable load drop as calculated in Eq. 3 to be equal to $(\frac{1}{\sqrt{2}})F_C$. Assuming the initial delamination behaviour and N=2 on the left hand side of Eq. 5, and multiple delaminations (N-1=3) and an unknown delamination size after the load drop on the right hand side, Eq. 5 can be solved for the delamination size;

$$\alpha \approx 0.14 \quad (6)$$

The actual delamination diameter can then be estimated to be about 5 mm for the Ref case and about 10 mm for the Ps case. These estimates appear to give a reasonable order of magnitude when compared to the maximum delamination sizes obtained experimentally, in table 2.

According to this simplified analysis, the delamination size should scale with the in-plane plate dimensions. The true scaled pair, that is the Ref and the Ps plates, match this ratio:

$$\frac{a_{Ps}}{a_{Ref}} = \begin{matrix} 2.00 & \textit{Theoretical} \\ 2.05 & \textit{Experimental} \end{matrix}$$

(the experimental values are given in Table 2). This delamination damage scaling due to transverse loading after critical load, reached for true scaled laminates, is consistent with a similar work carried out in [26] in which an averaged initial delamination size scaling factor of 2.18 was experimentally obtained based on three pairs of true scaled laminates.

By using the above approach, some useful insights into the scaling mechanisms involved in this experimental study can be obtained. However, this is still not able to capture the full nonlinear response of the laminate and the various damage mode magnitudes and interactions, as well as the boundary conditions,

across all the different laminate configurations. To achieve this the high-fidelity numerical models that are presented and validated in part 2 are required, where the damage is explicitly modelled by formulations based on combined stress and fracture energy criteria, and effects of nonlinearity, boundary conditions and delamination on the response of laminate under transverse loading are better captured.

4.5 Scaling of matrix cracks

The Is configuration has common features related to the Ss case in the sense that they have the same in-plane dimensions and the same ratio of ply thickness to characteristic length (width of supporting window). Hence, it is expected that these common physical features might be reflected by damage mechanisms. If one compares the difference in transverse cracks before and after the critical load for all cases (Figure 16), there is a similarity between Ref/Ps and Ss/Is cases. It can be seen that Ps and Ref have fewer long transverse cracks relative to their in-plane dimensions, while Is and Ss have multiple shorter transverse cracks. Overall the trend for matrix cracking is not strong and the events at the back face do not seem to play an important role in the development of delaminations, which cause the critical load drops (see numerical analysis in part 2).

5. Conclusions and Perspectives

This paper presents detailed experimental results explaining the mechanisms of damage development of laminated composite under transverse loading and providing data for validation of the numerical modelling strategies developed in part 2 of this study. Scaled indentation tests on quasi-isotropic composite plates were performed and a detailed assessment of the damage evolution was carried out through non-destructive techniques, such as ultrasonic scanning and X-ray computed tomography. Similar damage patterns were observed for all scaled plates. The first observable load drop in the global load-displacement curves was found to correspond to an unstable development of delamination at most interfaces, preceded by the presence of transverse cracks within the plies. A simplified model considering a circular homogeneous plate

with multiple delaminations was used to estimate the scaling of the main features of the plates' behavior at the first load drop. Further experimental data with additional scale factors for the various scaling parameters would be required in future work to fully understand the structural implications of damage scaling under transverse loading. The experiments presented here are sufficient to validate high fidelity finite element models (see part 2), ensuring they are capable of capturing such scaling effects. A further investigation of structural scaling could then also be undertaken in a simulation or virtual testing environment.

In addition to the geometrical parameters, the relative variation of bending stiffness as a result of the different stacking sequences, the ply block thickness and the characteristic length also influence the scaling. The degree of geometric nonlinearity is another important factor, particularly affecting the amount of delamination and associated critical load. The tentative explanation of the scaling given here based on simplified models is further investigated by the detailed numerical models presented in part 2. The simulated evolution of each degradation mechanism and its scaling with the plate characteristics give further insight to the scaling effects observed experimentally and helps to explain the experimental results in more detail, beyond the simplified models used in this paper.

Acknowledgements

The authors gratefully acknowledge the valuable technical discussions with Professor Hiroshi Suemasu, of the University of Sophia, on the analytical formulations used for this study.

References

[1] Wisnom MR, Hallett SR. The role of delamination in strength, failure mechanism and hole size effect in open hole tensile tests on quasi-isotropic laminates. Composites Part A: Applied Science and Manufacturing 2009;40:335–42. doi:10.1016/j.compositesa.2008.12.013.

[2] Chiao T, Reifsnider K, Sendeckyj G, Morgan R, Lien P, Takeda N, et al. Microscopic Observations of Cross Sections of Impacted Composite Laminates. Journal of Composites Technology and Research 1982;4:40. doi:10.1520/CTR10762J.

[3] Xu L. Interaction between matrix cracking and edge delamination in composite laminates. Composites Science and Technology 1994;50:469–78. doi:10.1016/0266-3538(94)90055-8.

[4] O'Higgins RM, McCarthy MA, McCarthy CT. Comparison of open hole tension characteristics of high strength glass and carbon fibre-reinforced composite materials. Composites Science and Technology 2008;68:2770–8. doi:10.1016/j.compscitech.2008.06.003.

[5] Green BG, Wisnom MR, Hallett SR. An experimental investigation into the tensile strength scaling of notched composites. Composites Part A: Applied Science and Manufacturing 2007;38:867–78. doi:10.1016/j.compositesa.2006.07.008.

[6] Mollenhauer D, Iarve E V., Kim R, Langley B. Examination of ply cracking in composite laminates with open holes: A moire interferometric and numerical study. Composites Part A: Applied Science and Manufacturing 2006;37:282–94. doi:10.1016/j.compositesa.2005.06.004.

[7] Tay T. Characterization and analysis of delamination fracture in composites: An overview of developments from 1990 to 2001. Applied Mechanics Reviews 2003;56:1. doi:10.1115/1.1504848.

[8] Hallett SR, Green BG, Jiang W-G, Cheung KH, Wisnom MR. The open hole tensile test: a challenge for virtual testing of composites. International Journal of Fracture 2009;158:169–81. doi:10.1007/s10704-009-9333-8.

[9] Abisset E, Daghia F, Ladevèze P. On the validation of a damage mesomodel for laminated composites by means of open-hole tensile tests on quasi-isotropic laminates. Composites Part A: Applied Science and Manufacturing 2011;42:1515–24. doi:10.1016/j.compositesa.2011.07.004.

[10] Van der Meer FP, Sluys LJ, Hallett SR, Wisnom MR. Computational modeling of complex failure mechanisms in laminates. Journal of Composite Materials 2011;46:603–23. doi:10.1177/0021998311410473.

[11] Wisnom MR, Hallett SR, Soutis C. Scaling Effects in Notched Composites. Journal of Composite Materials 2009;44:195–210. doi:10.1177/0021998309339865.

[12] Wisnom MR, Khan B, Hallett SR. Size effects in unnotched tensile strength of unidirectional and quasi-isotropic carbon/epoxy composites. Composite Structures 2008;84:21–8. doi:10.1016/j.compstruct.2007.06.002.

[13] ASTM standard D7136 / D7136M. Standard Test Method for Measuring the Damage Resistance of a Fiber-Reinforced Polymer Matrix Composite to a Drop-Weight Impact Event 2003. doi:10.1520/D7136_D7136M-12.

[14] Olsson R. Impact Response of Composite Laminates: A Guide to Closed Form Solutions. Aeronautical Research Institute of Sweden; 1993.

[15] Swanson SR. Limits of quasi-static solutions in impact of composite structures. Composites Engineering 1992;2:261–7. doi:10.1016/0961-9526(92)90009-U.

[16] Kwon YS, Sankar B V. Indentation-flexure and low-velocity impact damage in graphite epoxy laminates. Journal of Composites Technology and Research 1993;15:101. doi:10.1520/CTR10361J.

[17] Abrate S. Impact on composite structures. Cambridge University Press; 2005.

[18] Guinard S, Allix O, Guedradegeorges D, Vinet a. A 3D damage analysis of low-velocity impacts on laminated composites. Composites Science and Technology 2002;62:585–9. doi:10.1016/S0266-3538(01)00153-1.

[19] Bouvet C, Rivallant S, Barrau JJ. Low velocity impact modeling in composite laminates capturing permanent indentation. Composites Science and Technology 2012;72:1977–88. doi:10.1016/j.compscitech.2012.08.019.

[20] Fuoss E, Straznicky P, Poon C. Effects of stacking sequence on the impact resistance in composite laminates—Part 1: parametric study. Composite Structures 1998;8223.

[21] Chen P, Shen Z, Xiong J, Yang S, Fu S, Ye L. Failure mechanisms of laminated composites subjected to static indentation. Composite Structures 2006;75:489–95. doi:10.1016/j.compstruct.2006.04.087.

[22] González EV, Maimí P, Camanho PP, Lopes CS, Blanco N. Effects of ply clustering in laminated composite plates under low-velocity impact loading. Composites Science and Technology 2011;71:805–17. doi:10.1016/j.compscitech.2010.12.018.

[23] Hitchen SA, Kemp RMJ. The effect of stacking sequence on impact damage in a carbon fibre/epoxy composite. Composites 1995;26:207–14. doi:10.1016/0010-4361(95)91384-H.

[24] Aymerich F, Dore F, Priolo P. Simulation of multiple delaminations in impacted cross-ply laminates using a finite element model based on cohesive interface elements. Composites Science and Technology 2009;69:1699–709. doi:10.1016/j.compscitech.2008.10.025.

[25] Saito H, Morita M, Kawabe K, Kanesaki M, Takeuchi H, Tanaka M, et al. Effect of ply-thickness on impact damage morphology in CFRP laminates. Journal of Reinforced Plastics and Composites 2011;30:1097–106. doi:10.1177/0731684411416532.

[26] Nettles A, Douglas M, Estes E. Scaling effects in carbon/epoxy laminates under transverse quasi-static loading. NASA Technical Report, NASA/TM-1999-209103 1999.

[27] Christoforou AP, Yigit AS. Characterization of impact in composite plates. Composite Structures 1998;43:15–24. doi:10.1016/S0263-8223(98)00087-7.

[28] Schoeppner G a., Abrate S. Delamination threshold loads for low velocity impact on composite laminates. Composites Part A: Applied Science and Manufacturing 2000;31:903–15. doi:10.1016/S1359-835X(00)00061-0.

[29] Yang FJ, Cantwell WJ. Impact damage initiation in composite materials. Composites Science and Technology 2010;70:336–42. doi:10.1016/j.compscitech.2009.11.004.

[30] Caprino G, Lopresto V. The significance of indentation in the inspection of carbon fibre-reinforced plastic panels damaged by low-velocity impact. Composites Science and Technology 2000;60:1003–12. doi:10.1016/S0266-3538(99)00196-7.

[31] Curtis PT, ROYAL AEROSPACE ESTABLISHMENT FARNBOROUGH (England). CRAG (Composite Research Advisory Group) Test Methods for the Measurement of the Engineering Properties of Fibre Reinforced Plastics. Defense Technical Information Center; 1988.

[32] O'Brien T, Johnston W, Toland G. Mode II interlaminar fracture toughness and fatigue characterization of a graphite epoxy composite material. NASA Technical Report, NASA/TM-2010-216838, 2010.

[33] Nettles A.T, Hodge A. J. The Impact Response of Carbon/Epoxy Laminates. NASA Technical Report NASA/TM-97-206317. 1997.

[34] Hou JP, Petrinic N, Ruiz C, Hallett SR. Prediction of impact damage in composite plates. Composites Science and Technology 2000;60:273–81. doi:10.1016/S0266-3538(99)00126-8.

[35] Sun X, Wisnom MR, Hallett SR. Interaction of inter- and intralaminar damage in scaled quasi-static indentation tests: Part 2 - Numerical Simulation. Submitted to Composite Structures 2015.

[36] Gan KW, Hallett SR, Wisnom MR. Measurement and modelling of interlaminar shear strength enhancement under moderate through-thickness compression. Composites Part A: Applied Science and Manufacturing 2013;49:18–25. doi:10.1016/j.compositesa.2013.02.004.

[37] Shivakumar KN, Elber W, Illg W. Prediction of Impact Force and Duration Due to Low-Velocity Impact on Circular Composite Laminates. Journal of Applied Mechanics 1985;52:674. doi:10.1115/1.3169120.

[38] Reddy JN. Mechanics of Laminated Composite Plates and Shells: Theory and Analysis, Second Edition. Taylor & Francis; 2004.

[39] Suemasu H, Majima O. Multiple Delaminations and their Severity in Nonlinear Circular Plates Subjected to Concentrated Loading. Journal of Composite Materials 1998;32:123–40. doi:10.1177/002199839803200202.

[40] Viot P, Ballère L, Guillaumat L, Lataillade J-L. Scale effects on the response of composite structures under impact loading. Engineering Fracture Mechanics 2008;75:2725–36. doi:10.1016/j.engfracmech.2007.03.001.

[41] Buckingham E. On Physically Similar Systems; Illustrations of the Use of Dimensional Equations. Physical Review 1914;4:345–76. doi:10.1103/PhysRev.4.345.

[42] Davies GAO, Robinson P, Robson J, Eady D. Shear driven delamination propagation in two dimensions. Composites Part A: Applied Science and Manufacturing 1997;28:757–65. doi:10.1016/S1359-835X(97)00015-8.

[43] Suemasu H, Majima O. Multiple Delaminations and their Severity in Circular Axisymmetric Plates Subjected to Transverse Loading. Journal of Composite Materials 1996;30:441–53. doi:10.1177/002199839603000402.

[44] Olsson R, Donadon M V., Falzon BG. Delamination threshold load for dynamic impact on plates. International Journal of Solids and Structures 2006;43:3124–41. doi:10.1016/j.ijsolstr.2005.05.005.

[45] Suemasu H, Wisnom MR, Sun XC, Hallett SR. Damage Estimation in Nonlinear Laminates Subjected to a Transverse Concentrated Load. 20th International Conference on Composite Materials, 2015, p. 19–24.

[46] Nettles A, Douglas M. A comparison of quasi-static indentation to low-velocity impact. NASA Technical Report NASA/TP-2000-210481,2000.

[47] Yokozeki T, Kuroda A, Yoshimura A, Ogasawara T, Aoki T. Damage characterization in thin-ply composite laminates under out-of-plane transverse loadings. Composite Structures 2010;93:49–57. doi:10.1016/j.compstruct.2010.06.016.

Figures

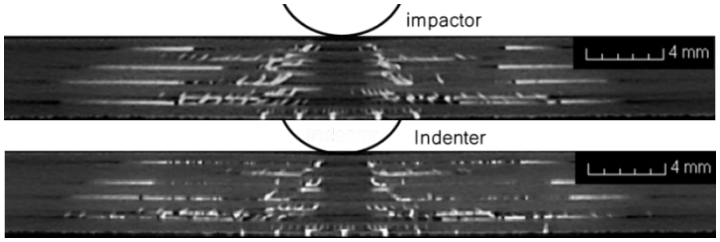

Figure 1. X-ray images of cross-section of two identical Ps laminates (Ply-blocked scaling) comparing damage extent caused by dynamic low-velocity impact (upper) and quasi-static indentation (lower).

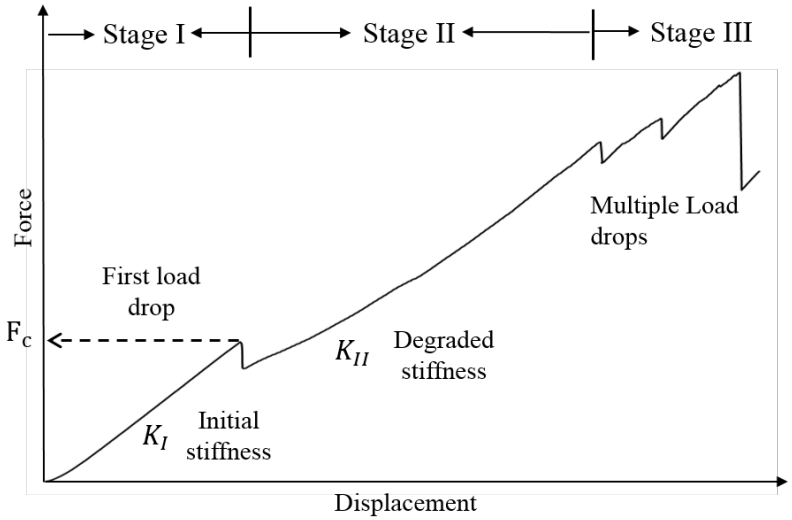

Figure 2. Schematic of load-displacement curve of typical quasi-static indentation test on quasi-isotropic composite plate.

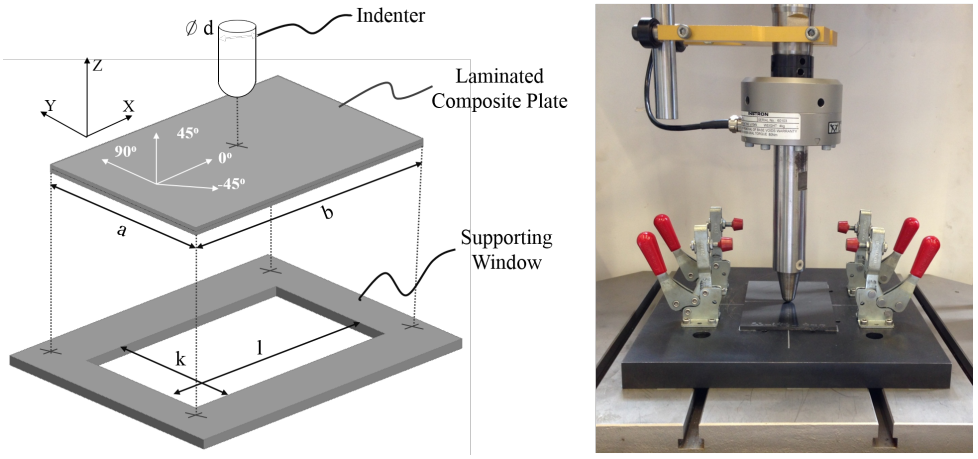

Figure 3 Experimental configuration for the static indentation tests.

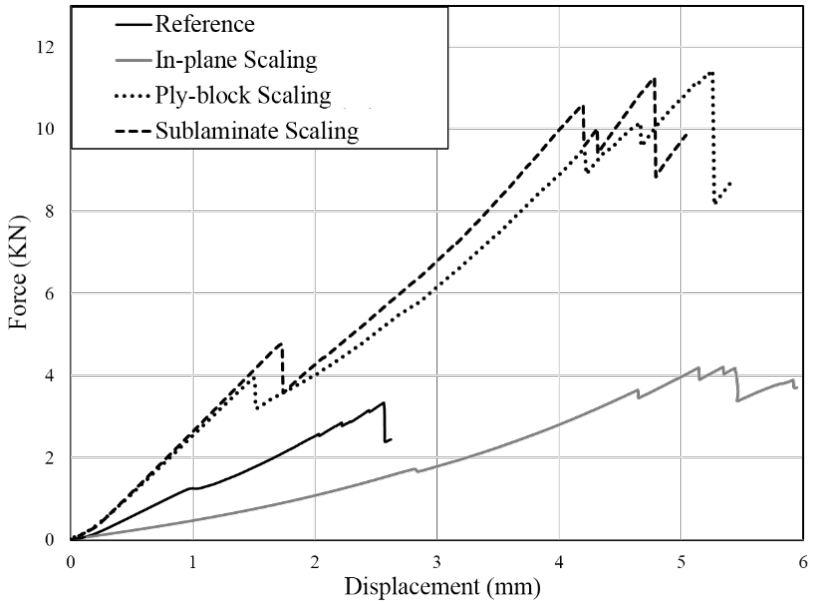

Figure 4. Load-displacement curves for the four types of specimens.

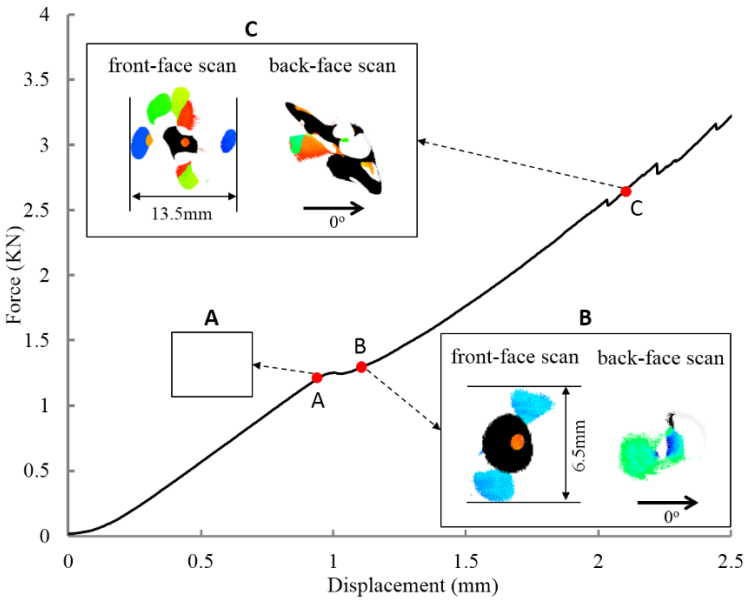

Figure 5. Representative global load-displacement curve and C-scan images depicting the overall delamination width for Reference case.

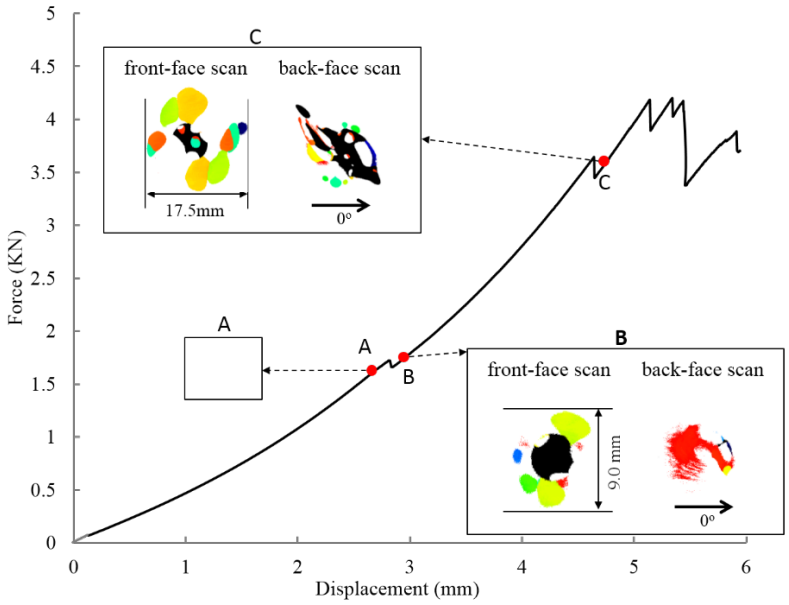

Figure 6. Representative global load-displacement curve and C-scans depicting the overall delamination width for In-plane scaled plate.

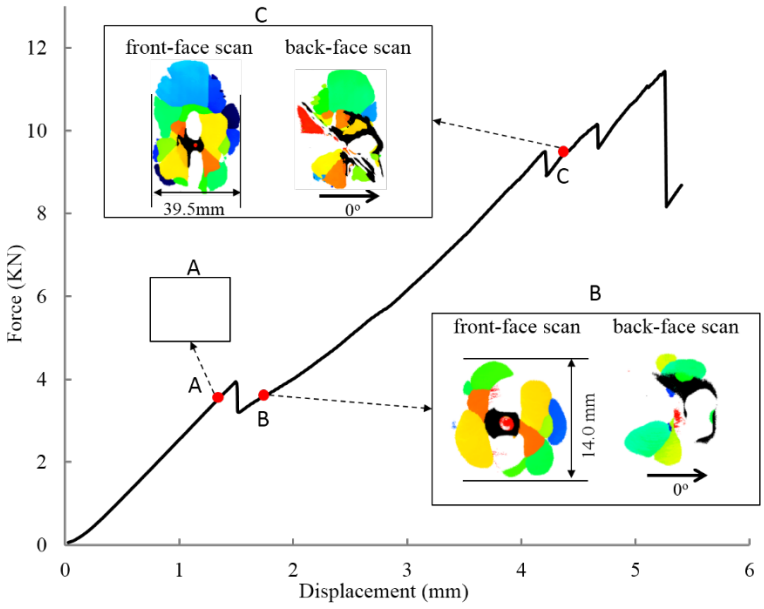

Figure 7 Representative global load-displacement curve and C-scans depicting the overall delamination width for Ply-block scaled plate.

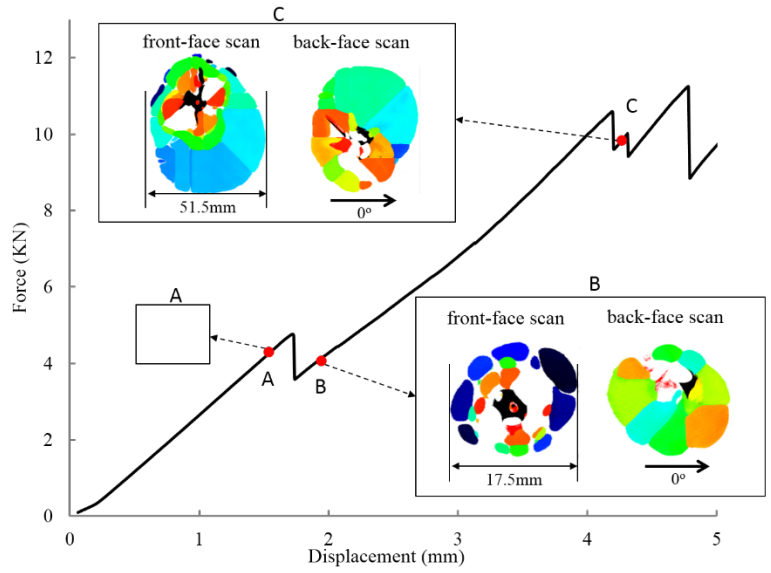

Figure 8. Representative global load-displacement curve and C-scans depicting the overall delamination width for sublaminate scaled plate.

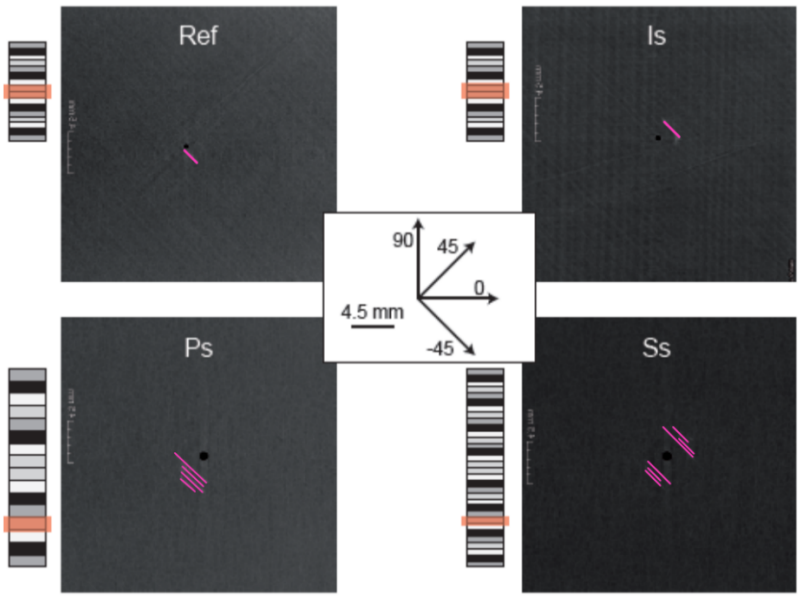

Figure 9. Uppermost transverse cracks in each of the four test cases before the first load drop. The location of the transverse crack in the thickness direction is marked on the left hand side of each image.

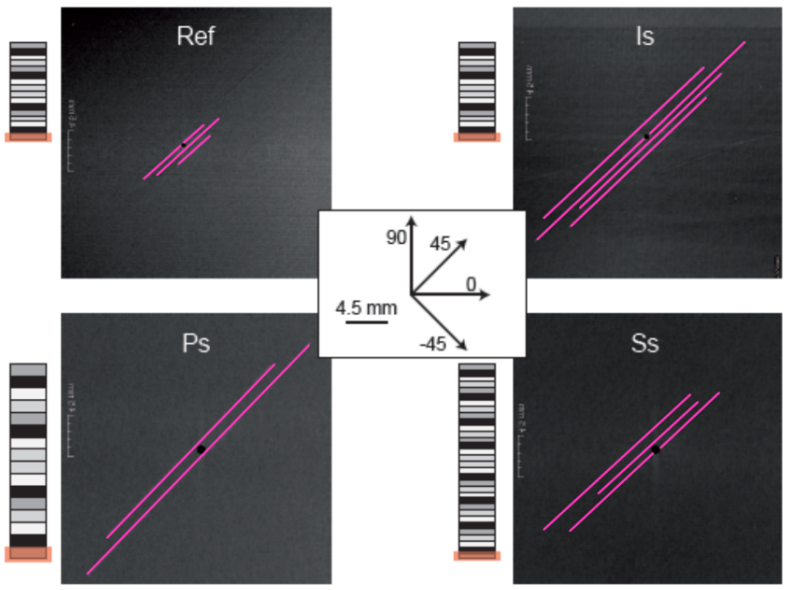

Figure 10. Transverse cracks in the bottom ply in each of the four test cases before the first load drop. The location of the transverse crack in the thickness direction is marked on the left hand side of each image.

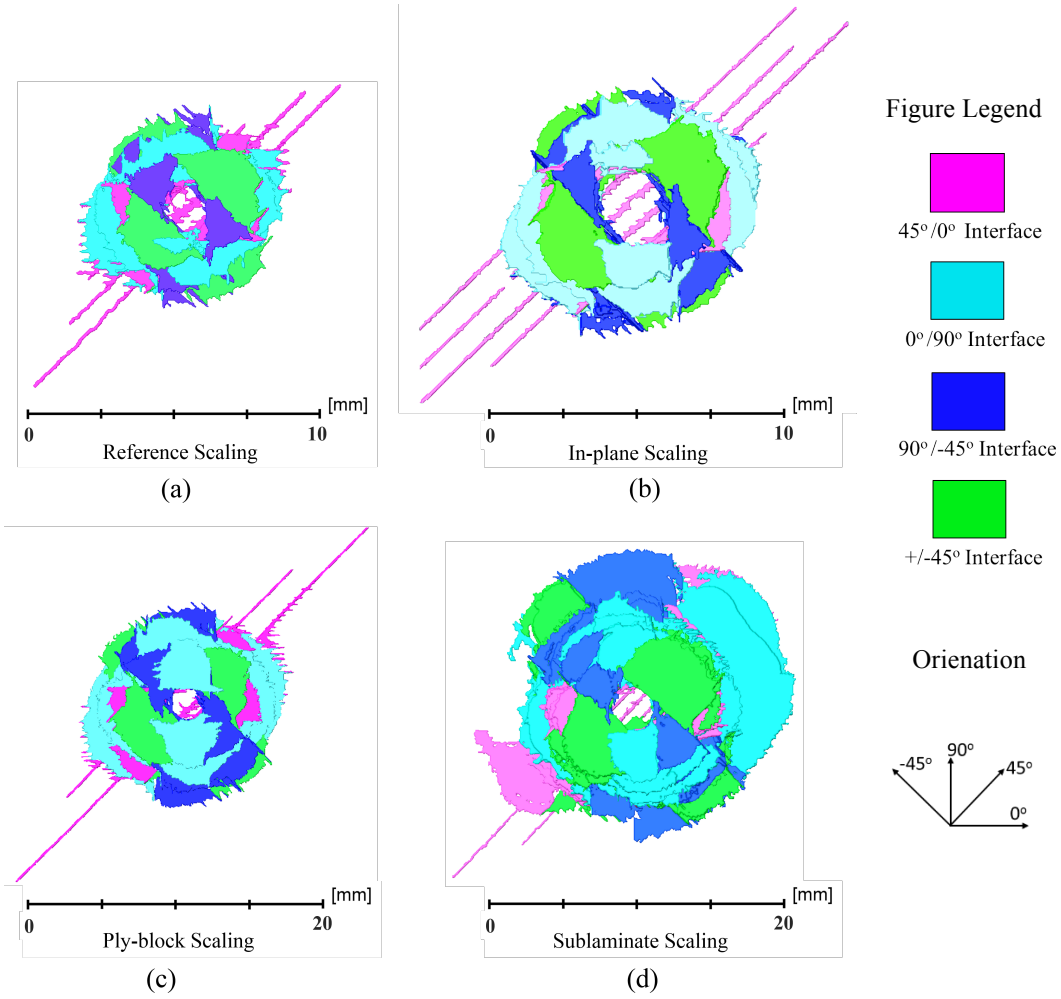

Figure 11. Post-processed 3D X-ray images for each type of specimen taken after the first load drop. Each interface with the same interface angle is coloured as shown in the figure legend.

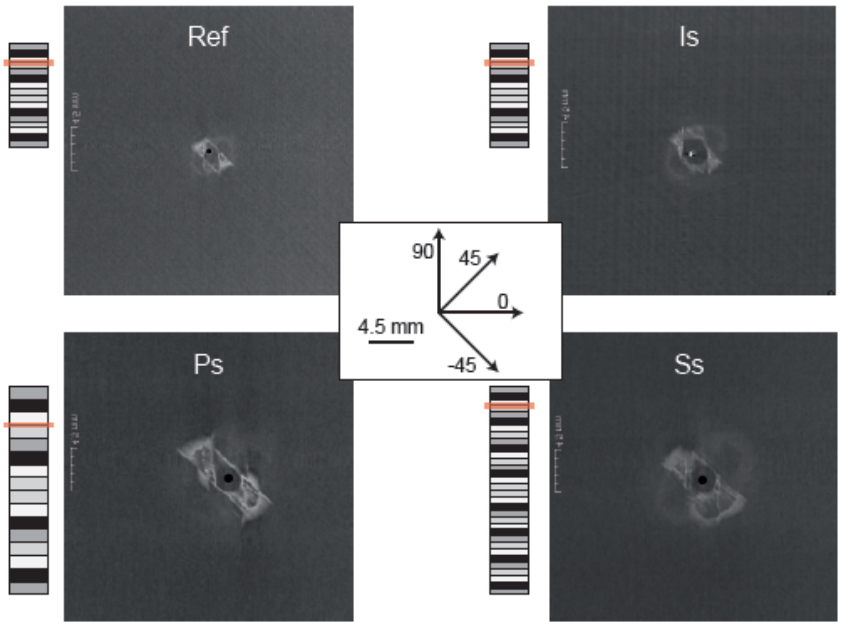

Figure 12. Delamination after the first load drop on the top 90/-45 interface for the four test cases. The location of this delamination in the thickness direction is marked on the left hand side of each image.

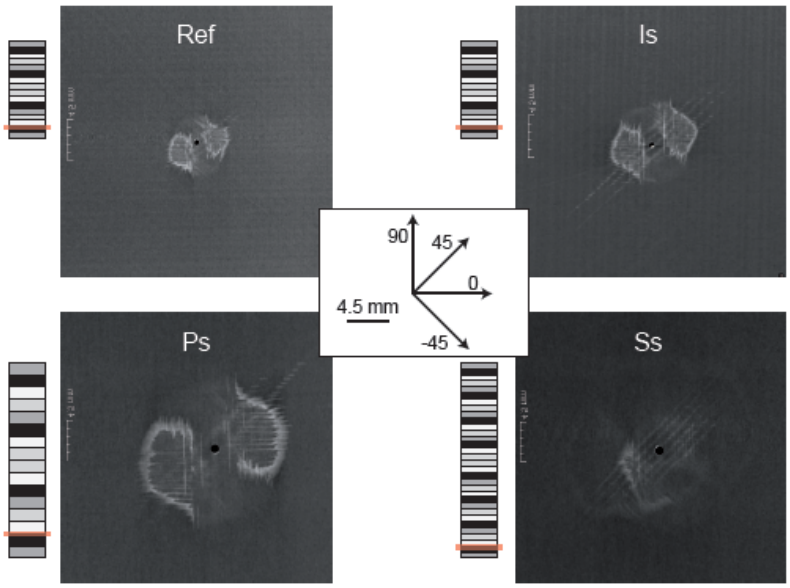

Figure 13. Delamination after the first load drop on the bottom 90/0 interface for the four test cases. The location of this delamination in the thickness direction is marked on the left hand side of each image.

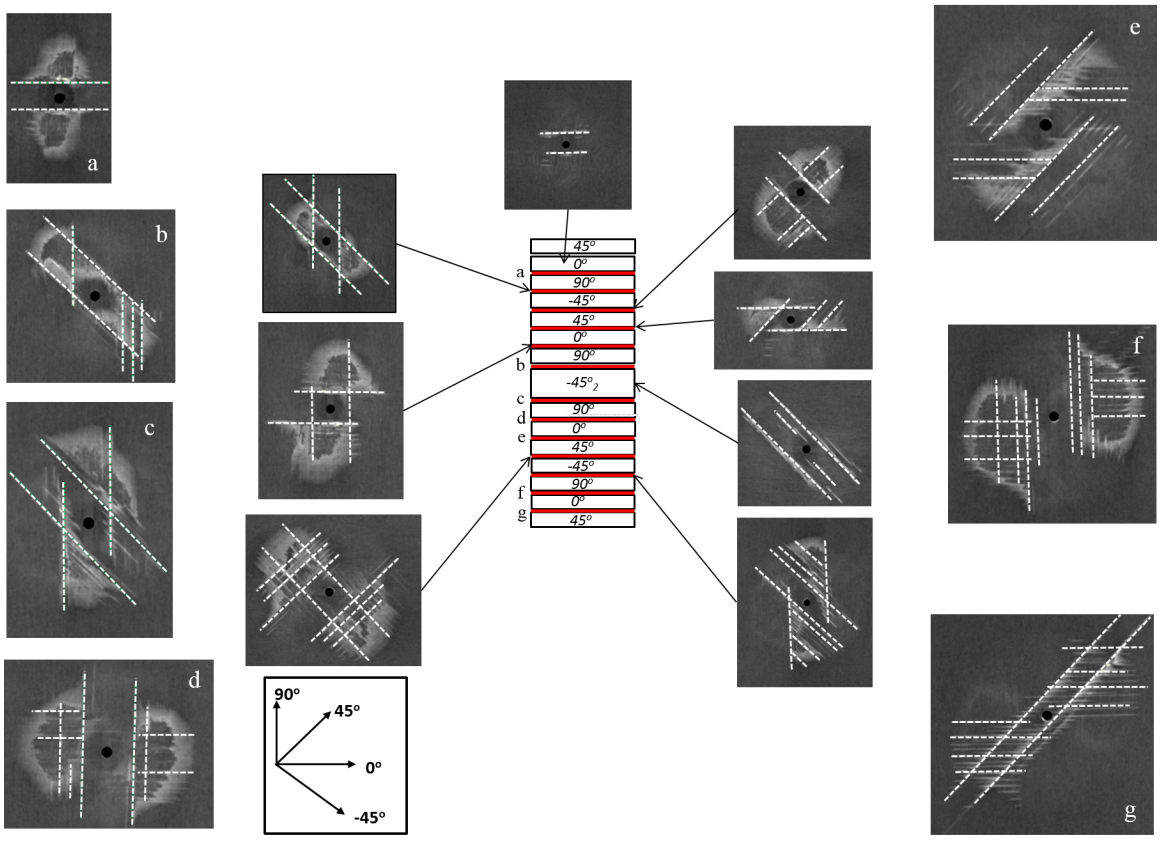

Figure 14. Collection of CT Images of delamination at each interface and neighbouring matrix crack in each ply for Ps case after first load drop, derived from X-ray CT scan. Distinctive matrix cracks are emphasised by green dashed lines. Each delamination is either pointed to the corresponding interface location, or from a to g.

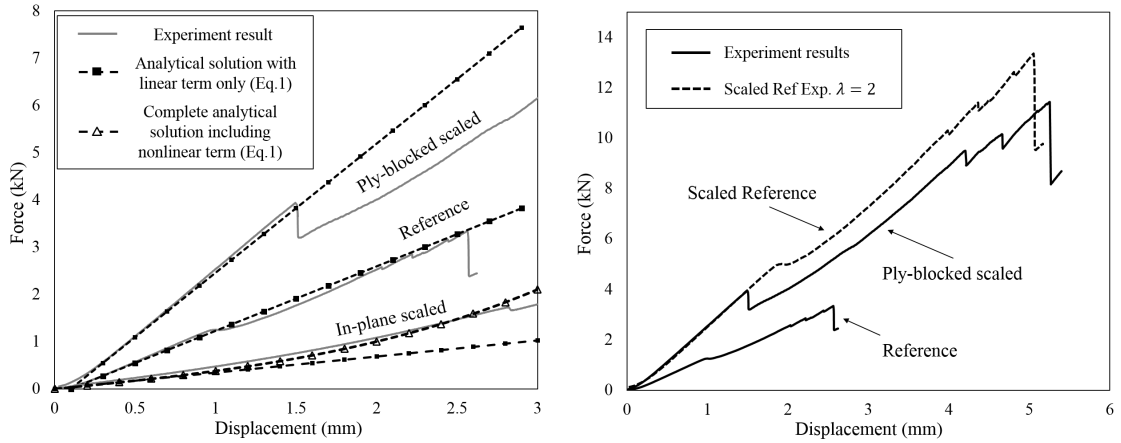

(a) (b)

Figure 15 Comparison of load-displacement plot between experimental and analytical solution for Ref, Ps and Is plate. (a) Comparison between linear analytical and experimental results for Ps, Ref and Is plate, A complete analytical solution with nonlinear term is included for the Is plate. (b) Comparison between the scaled-Ref plate (with scaling factor = 2), the Ps and the Ref plates.

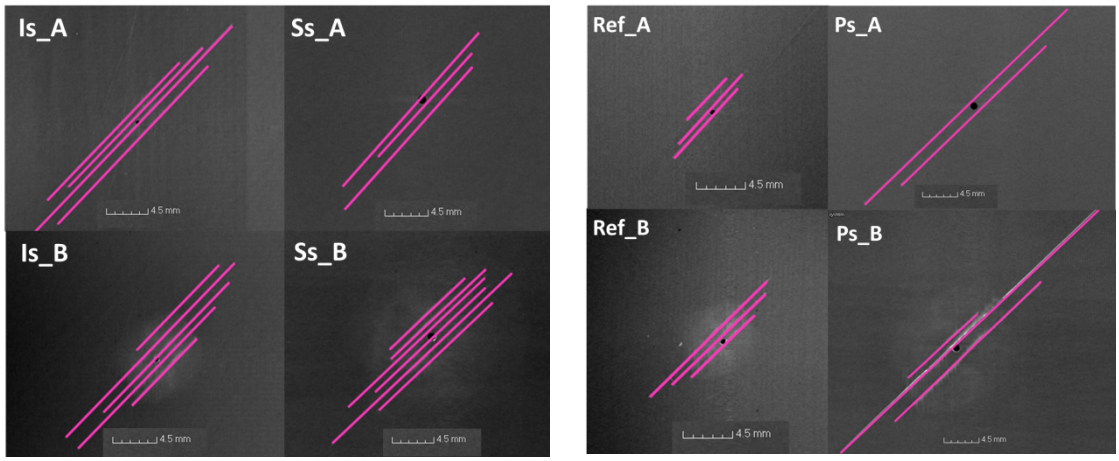

(a) (b)

Figure 16. Comparison of transverse bending cracks for all configurations before and after critical load. A indicates a specimen taken before load drop, and B indicates a specimen taken after the critical load.

Tables

Table 1 Characteristics of the tested specimen, where h_{plate} and h_{ply} is the plate overall cured thickness and nominal individual ply thickness. (Lay-up: [45m /0m /90m /−45m]ns with in-plane dimension 'a & b', and the indenter diameter is d).

Test case	m	n	h_{plate} (mm)	h_{ply} (mm)	In-plane dimensions a x b (mm)	Indenter diameter d (mm)
Reference (Ref)	1	2	2	0.125	75 × 50	8
In-plane scaling (Is)	1	2	2	0.125	150 × 100	16
Ply-block scaling (Ps)	2	2	4	0.25	150 × 100	16
Sublaminate scaling (Ss)	1	4	4	0.125	150 × 100	16

Table 2. Characteristic features of each scaled test.

Test case	**First Load Drop (FLD)**			**Max transverse crack length**		**Delamination after the first load drop**	
	Force (kN)	Displace-ment (mm)	level of load drop (%)	Before first load drop (mm)	After first load drop (mm)	Dia.[1] (mm)	Projected area (mm^2)
Reference (Ref)	1.28	1.0	3.54	9.0	14.6	6.6	34.2
In-plane scaling (Is)	1.70	2.8	3.74	31.5	24.3	8.5	57.1
Ply-block scaling (Ps)	3.96	1.5	21.0	35.5	45.7	13.5	142.5
Sublaminate scaling (Ss)	4.73	1.7	24.6	22.0	29.0	19.5	300.0

[1] The delamination diameters are calculated from projected areas, assuming circular delamination, instead of direct measurements.

Table 3. Comparison of experimental and analytical result of initial flexural stiffness of each laminate using Eq.1

Test case	Scaling parameter	Exp. initial stiffness (kN/mm) and scaling parameter	Analytical initial stiffness (kN/mm) and scaling parameter
Ref	*1*	1.47 (*1*)	1.36 (*1*)
Is	*0.25*	0.47 (*0.32*)	0.34(*0.25*)
Ps	*2*	2.87 (*1.95*)	2.73 (*2*)
Ss	*2*	2.98 (*2.02*)	

Table 4. Comparison of critical load for delamination obtained from experiment, analytical solution [32,42,43].

Test case	E_{eff} (GPa)	ν	G_{IIC} (N/mm)	h (mm)	F_C, Exp. (kN)	F_C, Theor. (kN)
Ref	42	0.3	0.8	2	1.28	1.61
Is	42			2	1.70	1.61
Ps	42			4	3.96	4.55
Ss	51.7			4	4.73	5.05